Conjugated Polymers Hot Paper

How to cite: *Angew. Chem. Int. Ed.* **2021**, *60*, 8189–8197
International Edition: doi.org/10.1002/anie.202015216
German Edition: doi.org/10.1002/ange.202015216

Efficient n-Doping of Polymeric Semiconductors through Controlling the Dynamics of Solution-State Polymer Aggregates

*Miao Xiong, Xinwen Yan, Jia-Tong Li, Song Zhang, Zhiqiang Cao, Nathaniel Prine, Yang Lu, Jie-Yu Wang, Xiaodan Gu, and Ting Lei**

Abstract: *Doping of polymeric semiconductors limits the miscibility between polymers and dopants. Although significant efforts have been devoted to enhancing miscibility through chemical modification, the electrical conductivities of n-doped polymeric semiconductors are usually below 10 $S\,cm^{-1}$. We report a different approach to overcome the miscibility issue by modulating the solution-state aggregates of conjugated polymers. We found that the solution-state aggregates of conjugated polymers not only changed with solvent and temperature but also changed with solution aging time. Modulating the solution-state polymer aggregates can directly influence their solid-state microstructures and miscibility with dopants. As a result, both high doping efficiency and high charge-carrier mobility were simultaneously obtained. The n-doped electrical conductivity of P(PzDPP-CT2) can be tuned up to 32.1 $S\,cm^{-1}$. This method can also be used to improve the doping efficiency of other polymer systems (e.g. N2200) with different aggregation tendencies and behaviors.*

Introduction

Doping of organic semiconductors is an important strategy to optimize their electronic properties.[1] Doping has been widely used to increase the charge-carrier density and reduce the charge injection/extraction barriers in organic electronic devices,[2] including organic field-effect transistors (OFETs),[3] organic light-emitting diodes (OLEDs),[4] and organic-photovoltaics (OPVs).[5] In organic thermoelectrics (OTEs), doping is always used to tune both electrical conductivity and the Seebeck coefficient to maximize the power factor.[6] To date, p-doped polymeric semiconductors have exhibited high electrical conductivities approaching or over 1000 $S\,cm^{-1}$,[7] whereas only a few n-doped conjugated polymers can show electrical conductivities over 1 $S\,cm^{-1}$.[8]

Since electrical conductivity ($\sigma = nq\mu$) is determined by charge-carrier density (n), elementary charge (q), and carrier mobility (μ), the key to improve electrical conductivity is to enhance charge-carrier density and mobility simultaneously. In the past decade, significant efforts have been devoted to the development of electron-deficient n-type polymeric semiconductors, and polymers with deep LUMO energy levels down to −4.3 eV have been reported.[9] However, further lowering the LUMO level is challenging, because strong electron-deficient building blocks are rare and chemical structures with LUMO levels lower than −4.4 eV may become unstable.[10] Air-stable strong n-dopant *N*-DMBI has a HOMO of −4.4 eV, but it can still dope conjugated polymers with a hydride or hydrogen atom transfer mechanism[11] (Figure 1a). Electron or hydride transfer requires close contact between polymer and dopant. Therefore, the miscibility between polymer and dopant is another key factor that greatly affects doping efficiency.[12] However, because of the strong interchain interactions of current state-of-art high-mobility conjugated polymers,[13] n-dopants can hardly mix well with these polymers, resulting in significant phase separation and low doping efficiency. Several molecular design strategies have been proposed to enhance the solid-state miscibility of conjugated polymers and dopants, such as replacing alkyl side chains with polar ethylene glycol side chains,[14] using twisted polymer building blocks,[1f] and incorporating "kinked" donor moieties.[1g] Enhancing miscibility indeed facilitate electron or hydride transfer with improved doping efficiency. However, these strategies always negatively influence the polymer interchain interactions, resulting in decreased mobility and eventually low conductivity.[6]

Polymer system is much more difficult to access the final equilibrium state than small molecules due to the entanglement of polymers chains. This dynamic feature makes polymers easily being trapped in different types of metastable states or unstable states during the phase-transition process.[15] Here we explore the dynamics of conjugated polymer aggregates in solution and their influences on doping. The n-type donor-acceptor (D-A) polymer, P(PzDPP-CT2),[16] with a LUMO energy level of −4.0 eV and a commonly used n-dopant, *N*-DMBI, are employed in this study (Figure 1a; Supporting Information, Figure S1). We found that the dynamics of the polymer aggregates can be utilized to enhance the doping efficiency of polymeric semiconductors, leading to controlled solid-state microstructures and miscibility with dopants. After carefully tuning the polymer aggregates in solution, the polymer-dopant miscibility and

[*] M. Xiong, Dr. X. Yan, J.-T. Li, Y. Lu, Prof. J.-Y. Wang, Prof. T. Lei
Key Laboratory of Polymer Chemistry and Physics of Ministry of Education, School of Materials Science and Engineering, College of Chemistry and Molecular Engineering, Peking University
Beijing 100871 (China)
E-mail: tinglei@pku.edu.cn
S. Zhang, Z. Cao, N. Prine, Prof. X. Gu
School of Polymer Science and Engineering, Center for Optoelectronic Materials and Devices, The University of Southern Mississippi
Hattiesburg, MS 39406 (USA)
Supporting information and the ORCID identification number(s) for the author(s) of this article can be found under: https://doi.org/10.1002/anie.202015216.

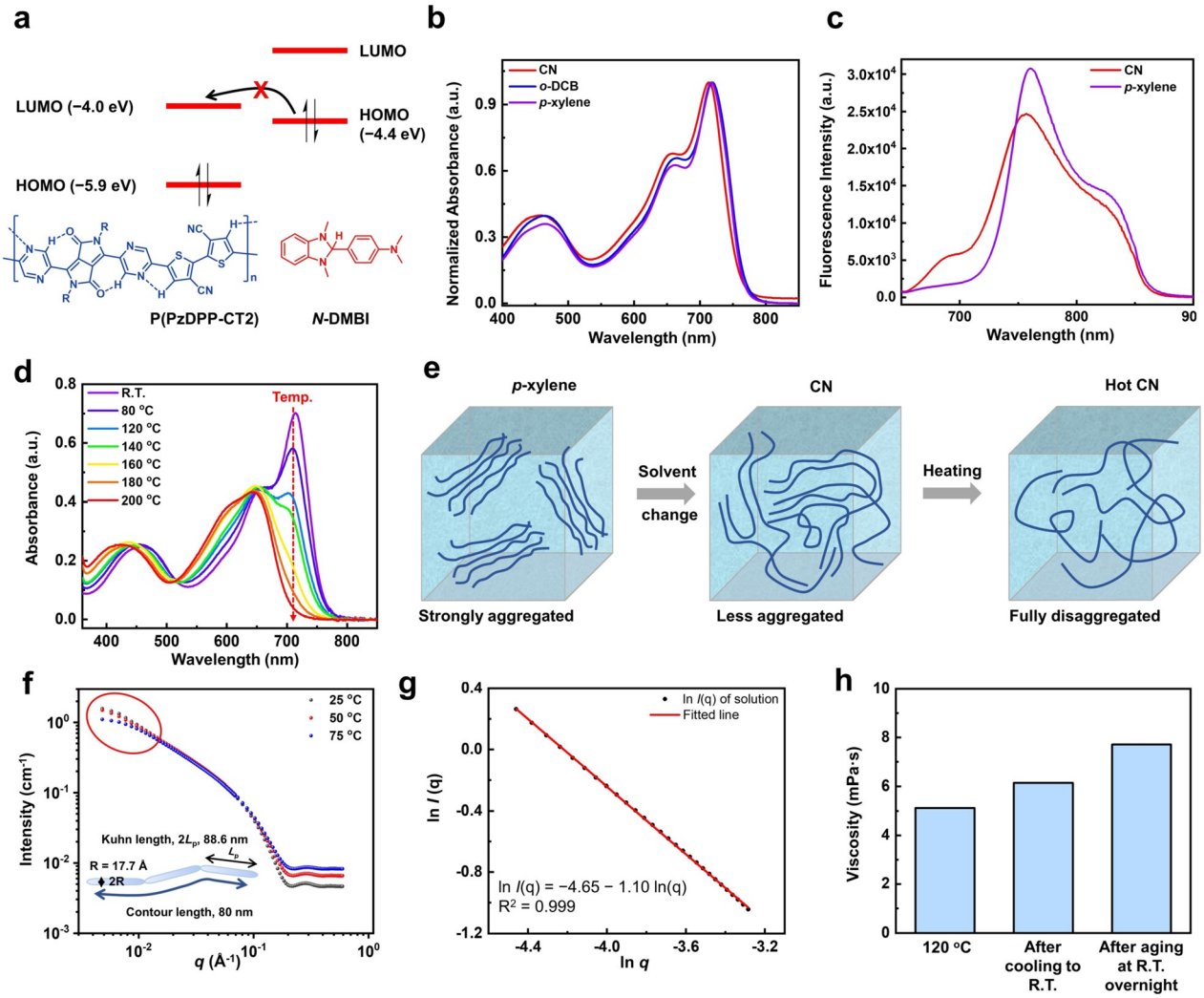

Figure 1. Solvent, temperature, and aging-time effects on the solution-state polymer aggregates. a) Chemical structures and energy levels of polymer P(PzDPP-CT2) and dopant *N*-DMBI. The electron transfer from *N*-DMBI to P(PzDPP-CT2) is unfavorable. Therefore, close contact between polymer and dopant is required. b) UV-vis-NIR absorption spectra of P(PzDPP-CT2) in *p*-xylene, *o*-DCB, and CN solution (1.0×10^{-5} M). c) Photoluminescence spectra of P(PzDPP-CT2) in dilute CN and *p*-xylene solutions with a concentration of 1.0×10^{-5} M. d) Temperature-dependent UV-vis-NIR absorption spectra of P(PzDPP-CT2) in CN solution (1.0×10^{-5} M). The red dotted line indicates the spectrum change as increasing the solution temperature. e) Illustration of changes of the solution-state aggregates by changing the solvent and temperature. f) Measured SANS data for P(PzDPP-CT2) in solution at 25 °C, 50 °C, and 75 °C. Inset: diagram of the 1D rod-like structure of the polymers in solution obtained from the analysis of the SANS data. Contour length, Kuhn length, and *R* are used to describe the shape of the polymer aggregates. g) Porod plot for the SANS data of P(PzDPP-CT2) in *o*-DCB at 75 °C. h) Viscosity change of P(PzDPP-CT2) solution in CN (3 mg mL^{-1}) at 120 °C, cooling to R.T. and aging at R.T. overnight. As the temperature decreased and the solution aged, the viscosity of the solution obviously increased.

doping efficiency in solid state can be modulated. As a result, P(PzDPP-CT2) exhibited one order of magnitude higher conductivities of up to 32.1 S cm^{-1}, among the highest value in solution-processed n-doped polymeric semiconductors. Using the same strategy, the electrical conductivity of N2200 was also doubled, suggesting that our method might be general for different types of conjugated polymers.

Results and Discussion

P(PzDPP-CT2) has a rigid and planar backbone because of its intramolecular hydrogen bonds. Such hydrogen bonds can be proved by DFT calculations and the single crystal structure of a PzDPP derivative (Figures S2 and S3). Through measuring the temperature-dependent absorption spectra of the polymer in different solvents (Figure S4), we screened out three solvents, *p*-xylene, 1,2-dichlorobenzene (*o*-DCB) and 1-chloronaphthalene (CN), for our study. The three solvents represent different disaggregation ability for the polymer. To determine the solution-state aggregation behavior of P(PzDPP-CT2), the UV-vis-NIR absorption spectra of the polymer solution (1.0×10^{-5} M) were measured at room temperature (R.T.) (Figure 1b). In all the solvents, P(PzDPP-CT2) shows the maximum absorption peak around 720 nm with a shoulder peak around 660 nm. In thin film, no

obvious spectral shift was observed after spin-coating from the three solvents (Figure S5a). However, in the solution state, the 720 nm peak of the polymer CN solution blue-shifted ≈5 nm compared to that of *o*-DCB and *p*-xylene. When varying the concentration of the CN solution from 1.0×10^{-5} M to 5.0×10^{-7} M, the 720 nm peak decreases more obviously than the 660 nm peak (Figure S5b). The observed changes of absorption spectra in different solvents and concentrations indicate that the polymer is aggregated in solution and the aggregation tendency is also different in different solvents[17] (Figure 1c; Figure S5). The aggregation is weaker in CN but stronger in *p*-xylene and *o*-DCB. This conclusion is also supported by the photoluminescence (PL) studies (Figure 1c; Figures S5 and S6). For D-A type conjugated polymers, distinguishing the aggregation type (J- or H- aggregation) is complicated. Significant amounts of characterization and computational studies are needed to fully understand the aggregation behaviors of the D-A polymers,[18] which is beyond the scope of this manuscript.

When the solution was heated from R.T. to 200 °C, the absorption peak at 720 nm decreased obviously and completely disappeared at 200 °C in CN (Figure 1d). The temperature-dependent absorption spectra showed that the aggregation peak at 720 nm dropped more severely in CN than in the other two solvents (Figure S4). In *o*-DCB, the aggregation peak did not disappear even at high temperatures of up to 200 °C (Figure S7). Thus, increasing solution temperature can reduce the extent of aggregation, and the polymers are more easily disaggregated in CN than the other two solvents (Figure 1e).

To explore the geometrical information of the polymer aggregates, small-angle neutron scattering (SANS) was employed. Due to the limitation of the temperature range and deuterated solvent choice (deuterated CN is not commercially available), we tested the polymer in deuterated *o*-DCB from 25 °C to 75 °C (Figure 1f). No Guinier region was observed at the lowest q, suggesting that the size of the scattering aggregates was out of the detection range.[19] After increasing the temperature to 75 °C, the decreased intensity in the low q range suggested that the size of the aggregates reduced at a higher temperature. The Porod exponent α can provide the geometrical information of polymer aggregates in solution. The Porod exponent from SANS data showed that the polymer aggregates have a rod-like structure with rigid chains[20] (Figure 1g; for further discussion, see Figure S8), which is different from traditional conjugated polymers with semi-rigid or lamellar structure in solution.[21] A flexible cylinder model is appropriate to describe the conjugated polymer in solution (Figure 1f). The contour length obtained from the SANS fitting is 80 nm, the Kuhn length ($2L_p$) and radius (R) are fitted to be 88.6 nm and 17.7 Å. The Kuhn length is significantly larger than that of P3HT[22] and P(DPP-T),[23] indicating that P(PzDPP-CT2) aggregates are rigid with poor chain flexibility in solution. Therefore, the polymer thin film devices are fabricated actually with "polymer aggregates", not "single polymer chains".

Furthermore, we found that the polymer aggregates were not only affected by temperature and solvents; they also kept changing after prolonged storage at room temperature. Since the large aggregates are out of the detection range of SANS, we used solution viscosity measurement to evaluate the change of the polymer aggregates. Cooling the polymer solution from 120 °C to R.T. leads to an increase of the solution viscosity from 5.12 to 6.14 mPa s. After aging the solution at R.T. overnight, the solution viscosity further increased to 7.71 mPa s (Figure 1h). The increase of solution viscosity indicates further polymer chain entanglements and the size increase of the polymer aggregates.[19] A slight change of the polymer absorption spectra was also observed after aging (Figure S9). These results suggest that the polymer aggregates are slowly changing after the temperature is equilibrated. Similar phenomena were also observed in a widely studied polymer, N2200, which also showed an obvious red shift in absorption spectra after aging overnight (Figure S10). This aging effect has not been reported to affect device performance. However, we will show that aging at R.T. can significantly affect the doping efficiency of polymeric semiconductors.

A widely-used n-dopant, *N*-DMBI,[24] was used to dope the polymer. The electrical conductivity of the n-doped polymer film was measured using the four-point probe method. Initially, we used our traditional doping method to prepare the polymer/dopant solution. We first heated the polymer solution to 120 °C to dissolve the polymer. After cooling the polymer solution to R.T. for about 30 min, *N*-DMBI was added. The mixture was directly spin-coated on a glass substrate with patterned gold electrodes. After annealing the as-casted film to activate the doping, the polymer film was ready for measurement. We screened the dopant/polymer ratios with different solvents (Figure 2a). The maximal conductivity of P(PzDPP-CT2) film prepared from *N*-DMBI/polymer *p*-xylene solution was 2.6 S cm^{-1}. For films prepared from *o*-DCB (60% *N*-DMBI/polymer ratio), the maximal conductivity reached 8.5 S cm^{-1}. After changing the solvent to CN, the maximal conductivity was further enhanced to 20.2 S cm^{-1}. These results suggest that the optimal *N*-DMBI/polymer ratio is around 60%, and CN is a better solvent.

During the experiment, we observed that after the polymer was dissolved under 120 °C, the solution cooling time and aging time seemed very critical for final device performance. Therefore, we cooled the polymer CN solution overnight and then added the dopants to the polymer solution (Figure 2b). Using this overnight cooled polymer and dopant solution, the prepared films only showed a maximal conductivity of 5.6 S cm^{-1}. With the same solution, the polymer/dopant mixture was heated to 120 °C for 1 h, and the prepared films showed a conductivity of 29.8 S cm^{-1}. After cooling the same solution at room temperature for 15 min, the conductivity of the prepared films slightly decreased to 27.6 S cm^{-1}. After a further 1 h cooling, the conductivity decreased to 19.2 S cm^{-1}, and after 2 h cooling, the conductivity decreased to 9.3 S cm^{-1}. Clearly, the conductivity of the polymer films depends on the cooling and aging time. After 30 min of cooling, the solution was already cooled to room temperature. However, we still observed noticeable changes of the film conductivity. Combined with the above aggregation behavior studies, these results further confirmed that the polymer

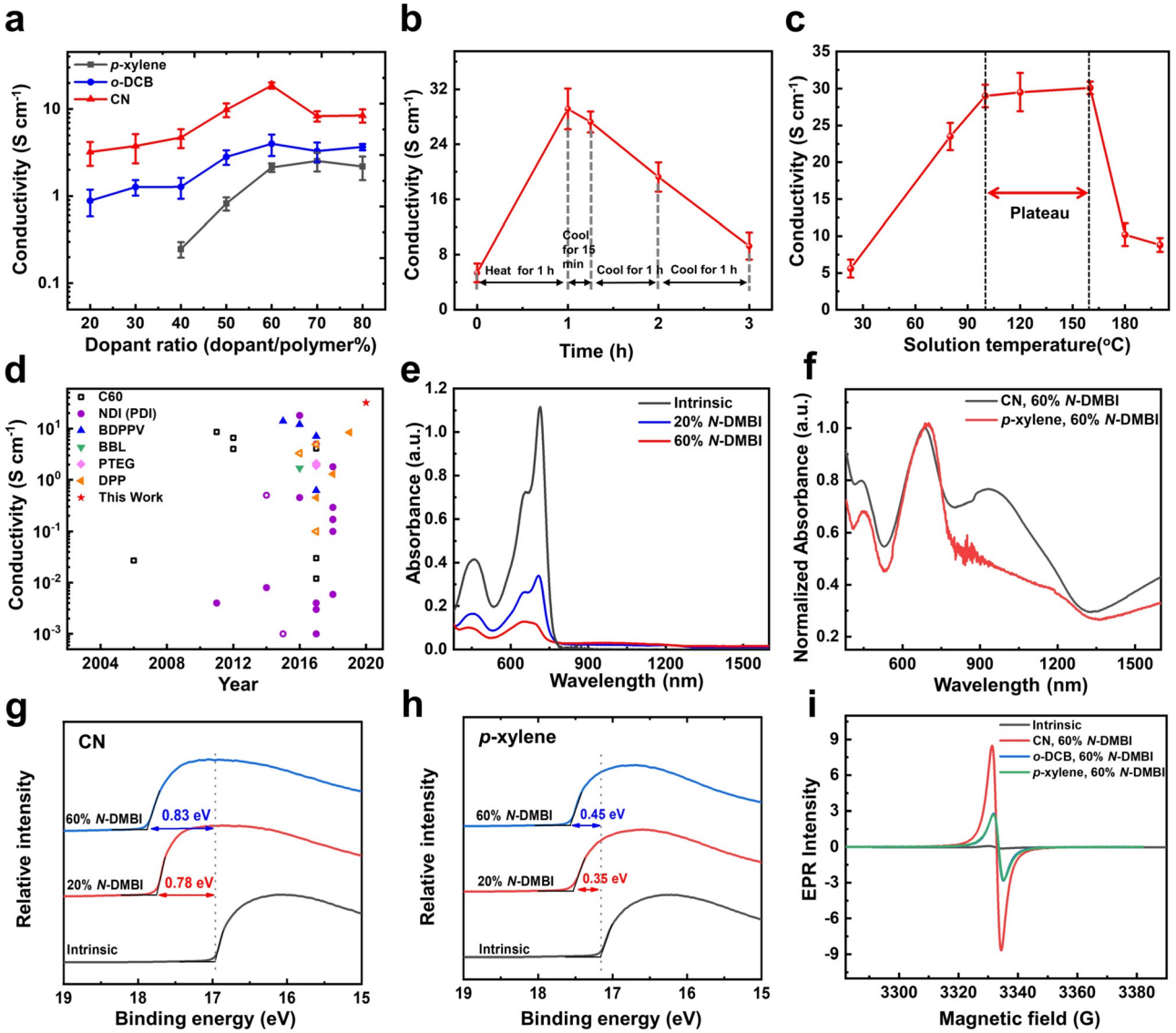

Figure 2. Modulating the solution-state aggregates to affect the doping efficiency and electrical conductivities of P(PzDPP-CT2). a) Conductivity of the doped polymers at different concentrations of *N*-DMBI in CN, *o*-DCB, and *p*-xylene; 14 devices were measured for each data point. The polymer solution and dopants were mixed at room temperature. b) The solution aging time dependent electrical conductivities of the doped polymer films. The mixture was heated at 120 °C for 1 h. After that, the solution was cooled at room temperature naturally for 15 min, 1 h, and 2 h. The films were prepared by spin coating and dried in vacuum, finally annealing at 120 °C for 2 h to activate the doping process. c) The conductivities of the doped polymer films prepared with the polymer/dopant solutions heated at different temperatures. d) Electrical conductivity comparison of the current state-of-the-art n-doped organic semiconductors. Each symbol represents a class of materials. P(PzDPP-CT2) exhibits the highest conductivity in n-doped polymeric semiconductors. Open symbols represent the small-molecule semiconductors. Solid symbols represent the polymeric semiconductors. e) UV-vis-NIR absorption spectra of intrinsic and *N*-DMBI doped polymers in CN after heating at 160 °C. f) UV-vis-NIR absorption spectra of doped P(PzDPP-CT2) films prepared with CN and *p*-xylene solutions. g,h) UPS binding energy of the pristine and the doped P(PzDPP-CT2) films prepared from CN and *p*-xylene solutions. The shifts of secondary electron cut-off (SECO) are marked. i) EPR signals of the intrinsic and the doped P(PzDPP-CT2) films cast from three solvents.

aggregates were still changing even after the temperature is at equilibrium (R.T.).

To explore the optimal heating temperature, we heated the polymer/dopant CN solution to different temperatures, and after a short time cooling (< 5 min), we spin-coated the solution onto the substrate. The conductivity of the polymer films changed obviously as varying the solution temperature (Figure 2c). When the solution temperature increased from R.T. to 100 °C, the film conductivity increased gradually from 5.6 to 28.8 $S cm^{-1}$. We observed a conductivity plateau at around 30 $S cm^{-1}$ in the temperature range from 100 °C to 160 °C. The highest conductivity reached 32.1 $S cm^{-1}$ (Figure 2d), which is the highest value in n-doped conjugated polymers. Then a sudden decrease of conductivities to < 10 $S cm^{-1}$ occurred in the temperature range from 160 °C to 200 °C.

Next, we will show that the conductivity improvement is due to the enhanced doping efficiency while keeping electron

mobility relatively high, and the sudden conductivity decrease can be attributed to the sudden mobility drop at high solution temperature. We first measured the absorption spectra of the polymer/dopant mixed solutions at R.T. or 160 °C. The solution only showed very weak new absorption bands that can be attributed to polaron/bipolarons even after heating (Figure 2e; Figure S11). In contrast, the doped polymer films showed strong polaron/bipolaron absorptions after annealing (Figure 2f; Figure S12). The polaron/bipolaron absorption of the high conductivity film prepared from CN was stronger than those films with much lower conductivities. These results indicate that the doping happens mainly in the solid state, not in solution. The ultraviolet photoelectron spectroscopy (UPS) secondary electron cut-off of the high conductivity polymer film prepared from CN solutions shifted 0.78 eV and 0.83 eV when doped with 20% *N*-DMBI and 60% *N*-DMBI, clearly larger than the values from *o*-DCB (0.59 eV and 0.75 eV) and *p*-xylene (0.35 eV and 0.45 eV) (Figure 2g,h; Figure S13). X-ray photoelectron spectroscopy (XPS) also showed that in high conductivity films, the peak area ratio between N-DMBI$^+$ and other N (1s) peaks was larger than that of the low conductivity films (Figure S14). The electron paramagnetic resonance (EPR) spectroscopy was used to evaluate the numbers of radicals in the polymer after doping. The calculated spin density of the films prepared from CN was approximately 1.83×10^{20} cm^{-3}, which was much larger than that of the films prepared from *o*-DCB and *p*-xylene solutions (Figure 2i; Table S1). All the results indicate that the higher conductivities of the polymer films are largely due to higher doping levels, and the efficient electron/hydride transfer from *N*-DMBI to the polymer majorly happens in the solid state.

Except for doping efficiency, charge-carrier mobility can also influence the electrical conductivity. To determine the solvent and temperature effects on mobilities, we evaluated the electron mobilities of the polymer films by field-effect transistors (FETs). Films prepared from *o*-DCB and *p*-xylene showed similar electron mobilities with 0.78 ± 0.07 cm^2 V^{-1} s^{-1} and 0.75 ± 0.14 cm^2 V^{-1} s^{-1}, respectively. Films prepared from CN showed slightly lower electron mobilities of 0.70 ± 0.05 cm^2 V^{-1} s^{-1} (Figure 3a,b; Figure S15). Recent studies have suggested that a few short-range interchain connections is enough to provide effective charge transport pathways for high mobility polymers.[25] Although the film prepared from CN had lower film crystallinity and less ordered molecular packing, the film might still have enough interchain short-range connections for efficient charge transport. Using CN as the solvent, the electron mobilities remained relatively stable over the temperature range from R.T. to 120 °C (Figure 3c). After increasing to 140 °C or higher temperature, the film mobilities began to decrease. Only half of the original values at 180–200 °C were observed. As demonstrated in the temperature-dependent absorption spectrum studies, the polymer can be completely disaggregated at high temperature. Therefore, the falling of the mobility at high temperature might be

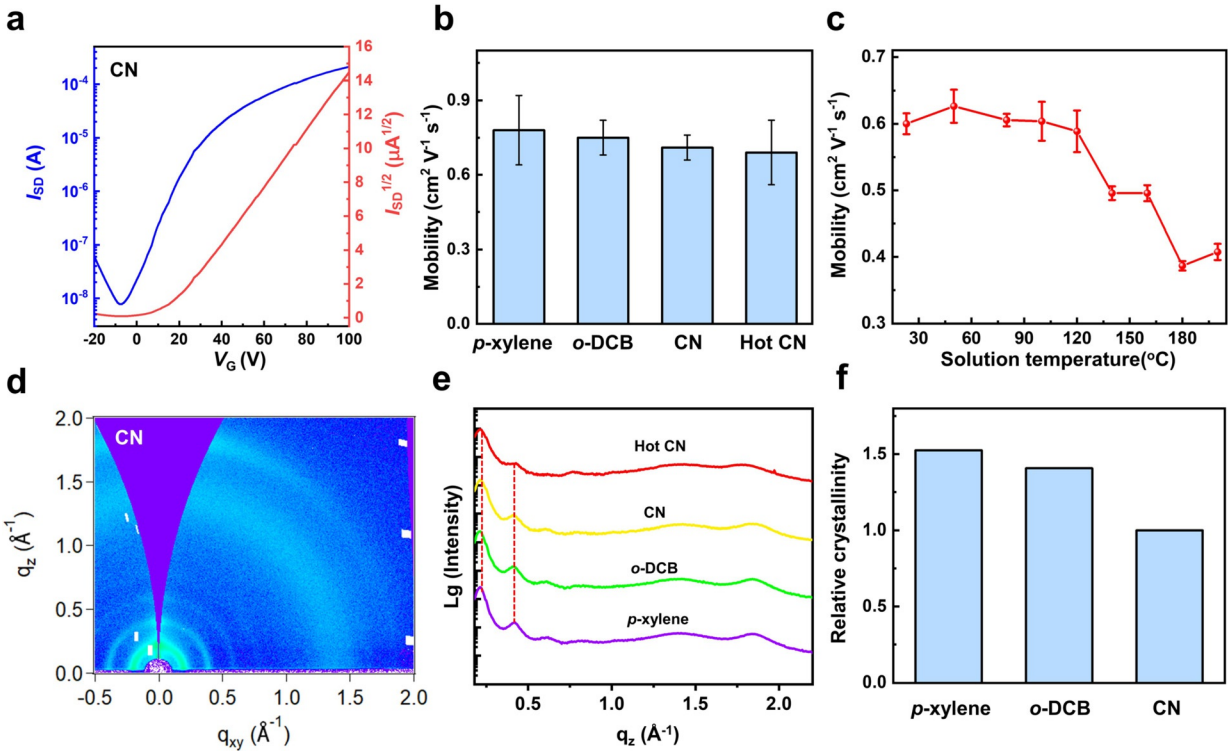

Figure 3. Charge-carrier transport and solid-state microstructure studies for the films prepared from different conditions. a) Typical transfer characteristics of P(PzDPP-CT2) films prepared from CN. Device configuration: $L = 5$ μm, $W = 100$ μm, and $C_i = 3.7$ nF cm^{-2}. b) Electron mobilities of polymer films prepared from different solvents (3 mg mL^{-1}). c) Electron mobilities of polymer films prepared from the polymer CN solution (3 mg mL^{-1}) heated at different temperatures. d) 2D-GIWAXS images of P(PzDPP-CT2) films prepared from CN (3 mg mL^{-1}). e) Out-of-plane GIWAXS plots of P(PzDPP-CT2) films prepared from *p*-xylene, *o*-DCB, CN, and hot CN (120 °C) solutions. f) The relative crystallinity of polymer films prepared from *p*-xylene, *o*-DCB, and CN extracted from the pole figure of (200) peak.

due to the destruction of interchain connections and thereby interchain charge transport.

Grazing-incidence wide-angle X-ray scattering (GIWAXS) was used to understand the film microstructures (Figure 3d,e; Figures S16 and S17). The lamellar packing (29.3 Å) and π-π stacking (3.38 Å) distances were the same for films prepared from the three solvents (Figure 3e). To compare the relative crystallinity of the films prepared from different solvents, the pole figure of (200) was extracted (Figure S18). The relative degree of crystallinity can be obtained by integrating the area below each curve, which indicated the film prepared from CN showed weaker crystallinity than the other two solvents (Figure 3f). These results suggest that using a good solvent (e.g., CN) and heating the solution to a higher temperature can reduce the solution-state aggregates and realize lower film crystallinity and less ordered molecular packing but still keep high charge-carrier mobilities.

GIWAXS data showed that 60% *N*-DMBI doped films prepared from different solvents had weaker crystallinity than the pristine film. As the *N*-DMBI concentration increasing, the lamellar packing and π-π stacking distances remained almost unchanged, suggesting that the dopants did not significantly alter molecular packing in the crystalline regions (Figures S19 and S20). AFM height images also proved that the doped polymer films with high conductivities showed good miscibility at high dopant/polymer ratios (60%) (Figure S21). In contrast, the low conductivity films prepared from *p*-xylene and *o*-DCB showed higher roughness and some dopant clusters (Figure S21j–l), indicating that phase separation happened in these low conductivity films.

We have shown that due to the strong interchain interactions of the D-A polymer, P(PzDPP-CT2) can adopt different polymer aggregation status in different solvents, at different temperatures, or after different aging times. Figure 4a illustrates the correlation between the solution-state aggregates and solid-state miscibility. Good solvent CN and higher temperature enable less polymer aggregation and interchain interactions. When the strongly aggregated polymers in solution disaggregate in a good solvent or by heating to a higher temperature, the dopants can be mixed well with the polymers. During the device fabrication (spin-coating), the polymer/dopants still keep good mixing due to the slow dynamics of polymer aggregates in solution, leading to good miscibility and efficient dopant-to-polymer electron/hydride transfer in solid state. The slow dynamics of the polymer aggregates can be supported by the slow viscosity increase of the polymer solution and the solution aging time dependent conductivity (Figures 1h and 2b). Cooling for a longer time, phase separation between polymers and dopants happens due to the strong aggregation tendency of the D-A type polymers, resulting in low doping efficiency. However, overheating the mixture can damage the interchain interactions of polymer chains and make the polymer aggregates excessively disaggregated, resulting in poor interchain connections, low charge-carrier mobilities, and decreased conductivities (160–200 °C range in Figure 2c). The disaggregation of the polymer chains at high temperature (160–200 °C) might limit the delocalization of the charges among aggregated chains and destabilize the polarons, which may further reduce the doping efficiency.[26] By controlling the solvent, temperature, and solution aging time, we can tune the aggregation status of the polymer and dopants. Even though the polymers get more aggregated during the temperature decreasing and solvent evaporating, the slow dynamics of the aggregates in solution still allow us to control the final solid-state miscibility and microstructures by controlling the starting polymer aggregation status, that is, the good mixing of the polymer/dopant aggregates in solution state can, to some extent, be inherited into solid state. The enhanced miscibility can be directly observed by AFM in combination with infrared-spectroscopy (AFM-IR)[27] (Figure 4b–d; Figure S22). We used the IR absorption of P(PzDPP-CT2) at 1660 cm^{-1} to explore the polymer and dopant distributions. The doped film prepared from CN with high conductivities showed a domain size of 28.4 nm, which is much smaller than those of the films prepared from *p*-xylene (50.2 nm) and *o*-DCB (48.8 nm). Therefore, the solid-state miscibility is indeed enhanced by controlling the polymer aggregation status in solution.

To further validate our assumptions, we performed AC-field Hall measurement for the n-doped films prepared from different solution temperature and aging times (Figure S23). The Hall mobility decreased as increasing the solution temperature. The film prepared from 120 °C solution showed increased charge-carrier concentration, which is an evidence for the high doping level after polymer chain is disentangled. The film prepared from 180 °C solution showed both decreased mobility and carrier concentration, which can be explained by the localization of charge carriers because of poor interchain connectivity. Under different solution aging time, longer aging time at R.T. led to lower charge-carrier concentrations and higher mobilities, suggesting that phase separation happened and interchain connection reconstructed during aging. All these results corroborate our proposed mechanism.

To test if our method is applicable for other polymeric semiconductors, the most widely studied D-A polymer N2200 was employed. Compared with P(PzDPP-CT2), N2200 showed different absorption spectra in *p*-xylene, *o*-DCB, and CN solution (Figure 5a,b). The aggregation behaviors of N2200 are different from P(PzDPP-CT2). N2200 is strongly aggregated in *p*-xylene, less aggregated in *o*-DCB, and fully disaggregated in CN.[28] The temperature-dependent absorption spectra of N2200 in *o*-DCB showed that the polymer aggregates can be modulated from weakly aggregated to fully disaggregated as increasing the temperature (Figure 5c). Thus, we choose *o*-DCB as the solvent for device fabrication. Similar to P(PzDPP-CT2), the electrical conductivity of the n-doped N2200 film prepared from *o*-DCB at R.T. is 7.5×10^{-3} $S\,cm^{-1}$, consistent with the values obtained by Chabynic et al. (8×10^{-3} $S\,cm^{-1}$).[29] After increasing the solution temperature to 70 °C, the electrical conductivity doubled to 1.7×10^{-2} $S\,cm^{-1}$ (Figure 5d). Further increasing the temperature leads to significantly decreased conductivities, similar to the case of P(PzDPP-CT2). In addition, the temperature-dependent conductivity of the low molecular weight P(PzDPP-CT2) was also measured, and a similar trend as the high molecular weight polymer was observed (Figure S24). Therefore, our

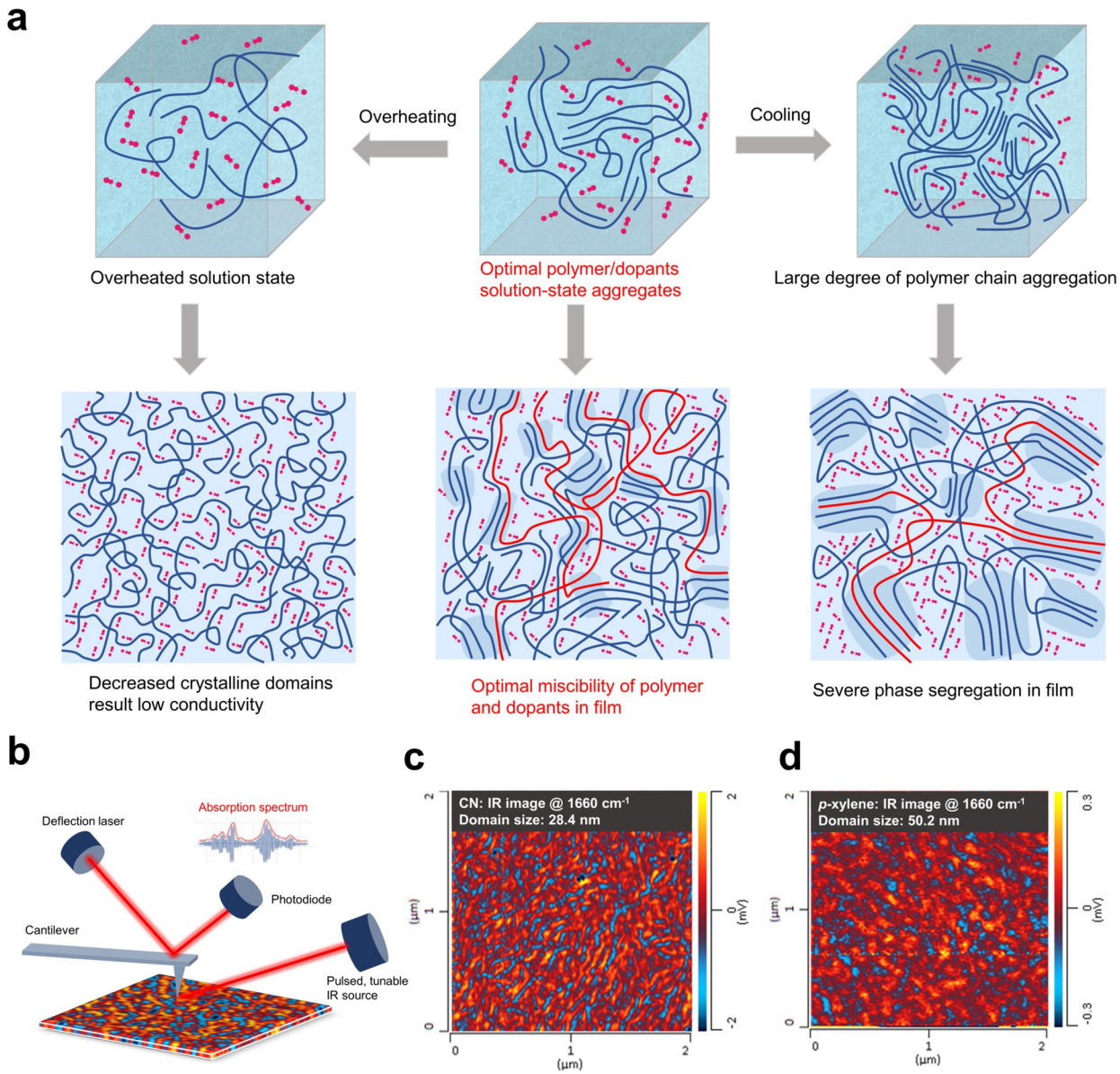

Figure 4. Controlling the solution-state polymer aggregates to achieve the optimal microstructures and miscibility with dopants in the solid state. a) Illustration of the aggregation status of P(PzDPP-CT2) and the distribution of *N*-DMBI in solutions and the corresponding film microstructures. Different starting solution-state aggregates can evolve to different solid-state morphologies during device fabrication. b) Illustration of the working principle for the AFM-IR system. c,d) AFM-IR absorption maps with the IR source tuned to 1660 cm^{-1} of the films prepared from CN and *p*-xylene.

method can be used for different types of polymeric semiconductors with different aggregation tendency.

Conclusion

To conclude, we observed that P(PzDPP-CT2) is strongly aggregated in solution, and the aggregates can be modulated by solvent, temperature, and aging time. Through understanding the slow dynamics of the solution-state polymer aggregates, we were able to modulate the polymer aggregates to a certain status in solution and control their solid-state microstructures and miscibility with dopants. The conductivity of P(PzDPP-CT2) can be tuned from 2.6 $S\,cm^{-1}$ to 32.1 $S\,cm^{-1}$ after exploring the dynamics of the polymer aggregates, which is a significant enhancement among doped conjugated polymers (Table S2). Since similar aggregation behaviors have been observed in many other polymeric semiconductors,[17,28,30] we also proved that our strategy to enhance the doping efficiency might be general for different polymer systems. We believe that the ease and broad applicability of our strategy will impact many device platforms requiring efficient doping of polymeric semiconductors.

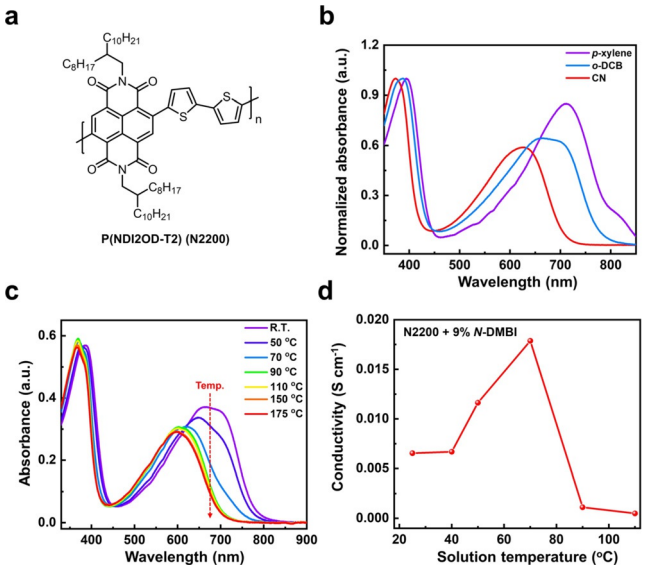

Figure 5. Modulating the solution-state aggregates of N2200 to enhance n-doping. a) Chemical structure of the polymer P(NDI2OD-T2), also known as N2200. b) UV-vis-NIR absorption spectra of N2200 in *o*-DCB, *p*-xylene, CN solution (1.0×10^{-5} M). c) Temperature-dependent UV-vis-NIR absorption spectra of N2200 in *o*-DCB solution (1.0×10^{-5} M). The red dotted line indicates the spectrum change as the solution temperature is increased. d) The electrical conductivities of 9% *N*-DMBI doped N2200 films prepared from *o*-DCB solutions heated at different temperatures.

Acknowledgements

This work is supported by the National Natural Science Foundation of China (22075001), the Key-Area Research and Development Program of Guangdong Province (2019B010934001), the Beijing Natural Science Foundation (2192020). X.Y. is thankful for the support of the China Postdoctoral Science Foundation (8206200018, 8206300146). The computational part is supported by the High-performance Computing Platform of Peking University. S.Z., N.P., and X.G. are thankful for financial support from the U.S. Department of Energy, Office of Science, Office of Basic Energy Science under the award number DE-SC0019361, which made the neutron and X-ray scattering, and AFM-IR measurements possible. A portion of this research was conducted at the Center for Nanophase Materials Sciences, which is a DOE Office of Science User Facility. A portion of this research used resources at the Spallation Neutron Source, a DOE Office of Science User Facility operated by the Oak Ridge National Laboratory.

Conflict of interest

The authors declare no conflict of interest.

Keywords: dynamic behaviors · n-doping · semiconductors · solution aggregates

[1] a) K. Xu, H. Sun, T.-P. Ruoko, G. Wang, R. Kroon, N. B. Kolhe, Y. Puttisong, X. Liu, D. Fazzi, K. Shibata, C.-Y. Yang, N. Sun, G. Persson, A. B. Yankovich, E. Olsson, H. Yoshida, W. M. Chen, M. Fahlman, M. Kemerink, S. A. Jenekhe, C. Müller, M. Berggren, S. Fabiano, *Nat. Mater.* **2020**, *19*, 738–744; b) B. Yurash, D. X. Cao, V. V. Brus, D. Leifert, M. Wang, A. Dixon, M. Seifrid, A. E. Mansour, D. Lungwitz, T. Liu, P. J. Santiago, K. R. Graham, N. Koch, G. C. Bazan, T.-Q. Nguyen, *Nat. Mater.* **2019**, *18*, 1327–1334; c) M. Schwarze, C. Gaul, R. Scholz, F. Bussolotti, A. Hofacker, K. S. Schellhammer, B. Nell, B. D. Naab, Z. Bao, D. Spoltore, K. Vandewal, J. Widmer, S. Kera, N. Ueno, F. Ortmann, K. Leo, *Nat. Mater.* **2019**, *18*, 242–248; d) V. A. Kolesov, C. Fuentes-Hernandez, W.-F. Chou, N. Aizawa, F. A. Larrain, M. Wang, A. Perrotta, S. Choi, S. Graham, G. C. Bazan, T.-Q. Nguyen, S. R. Marder, B. Kippelen, *Nat. Mater.* **2017**, *16*, 474–480; e) Y. Yamashita, J. Tsurumi, M. Ohno, R. Fujimoto, S. Kumagai, T. Kurosawa, T. Okamoto, J. Takeya, S. Watanabe, *Nature* **2019**, *572*, 634–638; f) E. E. Perry, C.-Y. Chiu, K. Moudgil, R. A. Schlitz, C. J. Takacs, K. A. O'Hara, J. G. Labram, A. M. Glaudell, J. B. Sherman, S. Barlow, C. J. Hawker, S. R. Marder, M. L. Chabinyc, *Chem. Mater.* **2017**, *29*, 9742–9750; g) Y. Shin, M. Massetti, H. Komber, T. Biskup, D. Nava, G. Lanzani, M. Caironi, M. Sommer, *Adv. Electron. Mater.* **2018**, *4*, 1700581.

[2] a) B. Lüssem, C. M. Keum, D. Kasemann, B. Naab, Z. N. Bao, K. Leo, *Chem. Rev.* **2016**, *116*, 13714–13751; b) C. G. Tang, M. C. Y. Ang, K.-K. Choo, V. Keerthi, J.-K. Tan, M. N. Syafiqah, T. Kugler, J. H. Burroughes, R.-Q. Png, L.-L. Chua, P. K. H. Ho, *Nature* **2016**, *539*, 536.

[3] M. Nikolka, I. Nasrallah, B. Rose, M. K. Ravva, K. Broch, A. Sadhanala, D. Harkin, J. Charmet, M. Hurhangee, A. Brown, S. Illig, P. Too, J. Jongman, I. McCulloch, J. L. Bredas, H. Sirringhaus, *Nat. Mater.* **2017**, *16*, 356–362.

[4] J. Blochwitz, M. Pfeiffer, T. Fritz, K. Leo, *Appl. Phys. Lett.* **1998**, *73*, 729–731.

[5] A. Dai, Y. Zhou, A. L. Shu, S. K. Mohapatra, H. Wang, C. Fuentes-Hernandez, Y. Zhang, S. Barlow, Y.-L. Loo, S. R. Marder, B. Kippelen, A. Kahn, *Adv. Funct. Mater.* **2014**, *24*, 2197–2204.

[6] B. Russ, A. Glaudell, J. J. Urban, M. L. Chabinyc, R. A. Segalman, *Nat. Rev. Mater.* **2016**, *1*, 16050.

[7] G. H. Kim, L. Shao, K. Zhang, K. P. Pipe, *Nat. Mater.* **2013**, *12*, 719–723.

[8] a) S. Wang, H. Sun, U. Ail, M. Vagin, P. O. Å. Persson, J. W. Andreasen, W. Thiel, M. Berggren, X. Crispin, D. Fazzi, S. Fabiano, *Adv. Mater.* **2016**, *28*, 10764–10771; b) J. Liu, G. Ye, B. van der Zee, J. Dong, X. Qiu, Y. Liu, G. Portale, R. C. Chiechi, L. J. A. Koster, *Adv. Mater.* **2018**, *30*, 1804290; c) J. Liu, Y. Shi, J. Dong, M. I. Nugraha, X. Qiu, M. Su, R. C. Chiechi, D. Baran, G. Portale, X. Guo, L. J. A. Koster, *ACS Energy Lett.* **2019**, *4*, 1556–1564.

[9] K. Shi, F. Zhang, C.-A. Di, T.-W. Yan, Y. Zou, X. Zhou, D. Zhu, J.-Y. Wang, J. Pei, *J. Am. Chem. Soc.* **2015**, *137*, 6979–6982.

[10] Q. Ye, J. Chang, K.-W. Huang, X. Shi, J. Wu, C. Chi, *Org. Lett.* **2013**, *15*, 1194–1197.

[11] B. D. Naab, S. Guo, S. Olthof, E. G. B. Evans, P. Wei, G. L. Millhauser, A. Kahn, S. Barlow, S. R. Marder, Z. Bao, *J. Am. Chem. Soc.* **2013**, *135*, 15018–15025.

[12] Y. Lu, J.-Y. Wang, J. Pei, *Chem. Mater.* **2019**, *31*, 6412–6423.

[13] a) Y. Liu, J. Zhao, Z. Li, C. Mu, W. Ma, H. Hu, K. Jiang, H. Lin, H. Ade, H. Yan, *Nat. Commun.* **2014**, *5*, 5293; b) M. Li, A. H. Balawi, P. J. Leenaers, L. Ning, G. H. L. Heintges, T. Marszalek, W. Pisula, M. M. Wienk, S. C. J. Meskers, Y. Yi, F. Laquai, R. A. J. Janssen, *Nat. Commun.* **2019**, *10*, 2867.

[14] a) J. Liu, L. Qiu, R. Alessandri, X. Qiu, G. Portale, J. Dong, W. Talsma, G. Ye, A. A. Sengrian, P. C. T. Souza, M. A. Loi, R. C.

Chiechi, S. J. Marrink, J. C. Hummelen, L. J. A. Koster, *Adv. Mater.* **2018**, *30*, 1704630; b) D. Kiefer, A. Giovannitti, H. Sun, T. Biskup, A. Hofmann, M. Koopmans, C. Cendra, S. Weber, L. J. A. Koster, E. Olsson, J. Rivnay, S. Fabiano, I. McCulloch, C. Müller, *ACS Energy Lett.* **2018**, *3*, 278 – 285.

[15] a) A. Keller, S. Z. D. Cheng, *Polymer* **1998**, *39*, 4461 – 4487; b) S. Z. D. Cheng, L. Zhu, C. Y. Li, P. S. Honigfort, A. Keller, *Thermochim. Acta* **1999**, *332*, 105 – 113.

[16] X. Yan, M. Xiong, J.-T. Li, S. Zhang, Z. Ahmad, Y. Lu, Z.-Y. Wang, Z.-F. Yao, J.-Y. Wang, X. Gu, T. Lei, *J. Am. Chem. Soc.* **2019**, *141*, 20215 – 20221.

[17] M. M. Nahid, A. Welford, E. Gann, L. Thomsen, K. P. Sharma, C. R. McNeill, *Adv. Electron. Mater.* **2018**, *4*, 1700559.

[18] C. Zhong, D. Bialas, F. C. Spano, *J. Phys. Chem. C* **2020**, *124*, 2146 – 2159.

[19] A. J. Clulow, E. P. Gilbert, P. Wolfer, P. L. Burn, I. R. Gentle, *Macromolecules* **2015**, *48*, 8331 – 8336.

[20] B. Hammouda, *Polym. Rev.* **2010**, *50*, 14 – 39.

[21] P. de la Iglesia, D. C. Pozzo, *Soft Matter* **2013**, *9*, 11214 – 11224.

[22] B. McCulloch, V. Ho, M. Hoarfrost, C. Stanley, C. Do, W. T. Heller, R. A. Segalman, *Macromolecules* **2013**, *46*, 1899 – 1907; Z. Cao, Z. Li, S. Zhang, L. Galuska, T. Li, C. Do, W. Xia, K. Hong, X. Gu, *Macromolecules* **2020**, *53*, 11142—11152.

[23] S. Zhang, M. U. Ocheje, L. Huang, L. Galuska, Z. Cao, S. Luo, Y.-H. Cheng, D. Ehlenberg, R. B. Goodman, D. Zhou, Y. Liu, Y.-C. Chiu, J. D. Azoulay, S. Rondeau-Gagné, X. Gu, *Adv. Electron. Mater.* **2019**, *5*, 1800899.

[24] P. Wei, J. H. Oh, G. Dong, Z. Bao, *J. Am. Chem. Soc.* **2010**, *132*, 8852 – 8853.

[25] R. Noriega, J. Rivnay, K. Vandewal, F. P. V. Koch, N. Stingelin, P. Smith, M. F. Toney, A. Salleo, *Nat. Mater.* **2013**, *12*, 1038 – 1044.

[26] J. Gao, E. T. Niles, J. K. Grey, *J. Phys. Chem. Lett.* **2013**, *4*, 2953 – 2957.

[27] A. Dazzi, C. B. Prater, *Chem. Rev.* **2017**, *117*, 5146 – 5173.

[28] R. Steyrleuthner, M. Schubert, I. Howard, B. Klaumünzer, K. Schilling, Z. Chen, P. Saalfrank, F. Laquai, A. Facchetti, D. Neher, *J. Am. Chem. Soc.* **2012**, *134*, 18303 – 18317.

[29] R. A. Schlitz, F. G. Brunetti, A. M. Glaudell, P. L. Miller, M. A. Brady, C. J. Takacs, C. J. Hawker, M. L. Chabinyc, *Adv. Mater.* **2014**, *26*, 2825 – 2830.

[30] a) M. Schubert, D. Dolfen, J. Frisch, S. Roland, R. Steyrleuthner, B. Stiller, Z. Chen, U. Scherf, N. Koch, A. Facchetti, D. Neher, *Adv. Energy Mater.* **2012**, *2*, 369 – 380; b) Y.-Q. Zheng, Z.-F. Yao, T. Lei, J.-H. Dou, C.-Y. Yang, L. Zou, X. Meng, W. Ma, J.-Y. Wang, J. Pei, *Adv. Mater.* **2017**, *29*, 1701072.

Manuscript received: November 14, 2020
Revised manuscript received: December 19, 2020
Accepted manuscript online: January 6, 2021
Version of record online: March 3, 2021

